Crustal thickness variations in northern Morocco

Flor de Lis Mancilla,[1,2] Daniel Stich,[1,2] José Morales,[1,2] Jordi Julià,[3,4] Jordi Diaz,[5] Antonio Pazos,[6] Diego Córdoba,[7] Javier A. Pulgar,[8] Pedro Ibarra,[9] Mimoun Harnafi,[10] and Francisco Gonzalez-Lodeiro[11]

Received 22 June 2011; revised 11 January 2012; accepted 12 January 2012; published 23 February 2012.

[1] During the TopoIberia experiment, a total of 26 seismic broadband stations were recording in northern Morocco, providing for the first time extended regional coverage for investigating structure and seismotectonics of the southern branch of the Betic-Rif arc, its foreland, and the Atlas domain. Here, we analyze *P*-to-*S* converted waves in teleseismic receiver functions to infer gross crustal properties as thickness and V_p/V_s ratio. Strong lateral variations of the crustal thickness are observed throughout the region. Crustal thicknesses vary between 22 and 44 km and display a simple geographic pattern that divides the study area into three domains: entire northwestern Morocco underlain by a thickened crust with crustal thicknesses between 35 and 44 km; northeastern Morocco affected by significant crustal thinning, with crustal thicknesses ranging from 22 to 30 km, with the shallowest Moho along the Mediterranean coast; and an extended domain of 27–34 km thick crust, farther south which includes the Atlas domain and its foreland regions. V_p/V_s ratios show normal values of ~1.75 for most stations except for the Atlas domain, where several stations give low V_p/V_s ratios of around 1.71. The very sharp transition from thick crust in northwestern Morocco to thin crust in northeastern Morocco is attributed to regional geodynamics, possibly the realm of present-day subcrustal dynamics in the final stage of western Mediterranean subduction. Crustal thicknesses just slightly above 30 km in the southern domain are intriguing, showing that high topography in this region is not isostatically compensated at crustal level.

Citation: Mancilla, F. de L., et al. (2012), Crustal thickness variations in northern Morocco, *J. Geophys. Res.*, *117*, B02312, doi:10.1029/2011JB008608.

1. Introduction

[2] The Gibraltar arc, which represents the westernmost end in the Mediterranean of the Alpine orogene, is formed by an arc-shaped mountain belt (Betic Cordillera in southern Spain and Rif in northern Morocco) surrounding the Alboran Sea. Evolution and present-day dynamics of the Gibraltar arc are topics that have received considerable attention in the last decades; however, the geodynamics of the region are still controversial [e.g., *Lonergan and White*, 1997; *Morales et al.*, 1999; *Seber et al.*, 1996; *Calvert et al.*, 2000; *Gutscher et al.*, 2002; *Duggen et al.*, 2004; *Faccenna et al.*, 2004; *Diaz et al.*, 2010]. The problem seems to reside in understanding the interplay between African-Eurasian plate convergence and regional-scale processes related to the evolution of the western Mediterranean. The solution to this problem appears to depend on a sound knowledge of deep lithospheric structure over the entire region. Data on deep lithospheric structure, however, have been comparably scarce in Algeria and Morocco, and fundamental parameters such as crustal thickness have to be either extrapolated from a few seismic profiles and single-station observations or estimated from the gravity field. Here, we analyze data from a recent temporal deployment of seismic broadband stations in order to obtain direct measurements of crustal thickness all over northern Morocco.

[3] Within the TopoIberia project (http://xeon.ictja.csic.es/IberArray), a large-scale multidisciplinary research initiative

[1]Instituto Andaluz de Geofísica, Universidad de Granada, Granada, Spain.
[2]Departamento de Física teórica y del Cosmos, Universidad de Granada, Granada, Spain.
[3]Departamento de Geofisica, Universidade Federal do Rio Grande do Norte, Natal, Brazil.
[4]Programa de Pós-graduacão em Geodinâmica e Geofísica, Universidade Federal do Rio Grande do Norte, Natal, Brazil.
[5]Institute of Earth Sciences "Jaume Almera," CSIC, Barcelona, Spain.
[6]Real Observatorio de La Armada, Cádiz, Spain.
[7]Departamento de Geofísica, Universidad Complutense de Madrid, Madrid, Spain.
[8]Departamento de Geología, Universidad de Oviedo, Oviedo, Spain.
[9]Instituto Geologico y Minero de Espana, Madrid, Spain.
[10]Institut Scientifique, Université Mohammed V Agdal, Rabat, Morocco.
[11]Departamento de Geodinámica, Universidad de Granada, Granada, Spain.

0148-0227/12/2011JB008608

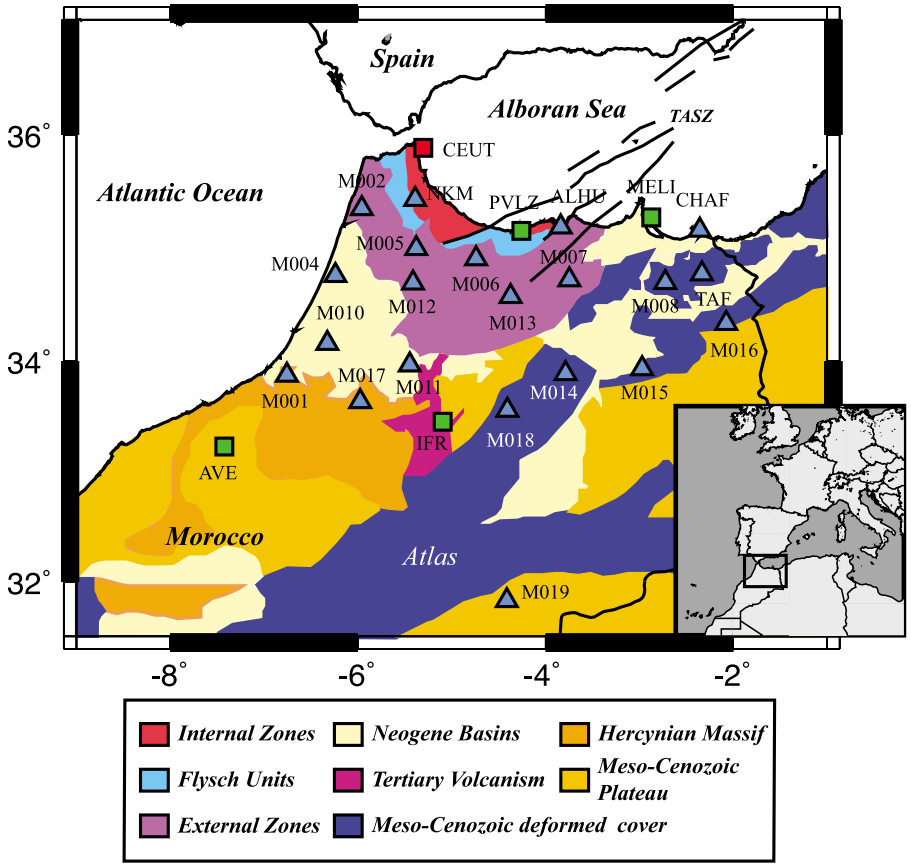

Figure 1. Geologic map of northern Morocco and position of the permanent and temporary broadband stations used in this study. Permanent stations of the western Mediterranean Network (http://geofon.gfz-potsdam.de/) are marked with green squares, one permanent station of the Instituto Andaluz de Geofisica (http://www.ugr.es/~iag/) is marked by a red square, and the temporary stations belonging to the TopoIberia deployment (http://xeon.ictja.csic.es/IberArray/) are marked with blue triangles. Thick black lines in the middle right of the map mark the position of the main faults of the trans-Alboran shear zone in the plotted area.

to investigate Earth's structure and dynamics in Spain and northern Morocco, 21 temporary seismic broadband stations were installed in northern Morocco, providing for the first time extended regional broadband coverage in this area. Most stations were active from 2007 to 2010 and provide good quality recordings of numerous teleseismic earthquakes from around the world. We use data from these temporary stations as well as from five permanent stations for receiver function analysis. The receiver function technique is a well-established seismology technique that permits extraction of information about the lithospheric structure from the analysis of converted seismic waves from three-component seismic recordings. We will show receiver function examples from the region that reveal clearly different characteristics of wave conversion beneath different stations and immediately point to strong lateral heterogeneity within the study area.

[4] We focus our attention on the conversion of *P* to *S* waves at the Moho interface (*Ps* phase) and the first multiple reverberations between surface and Moho (*PpPms* and *PpSms* + *PsPms* phases), corresponding to comparably clear arrivals in many of our receiver functions. The timing of these conversions is interpreted in terms of crustal thickness and the ratio between crustal *P* and *S* velocities beneath the stations. Finally, the good regional coverage and fairly dense station spacing (~60 km) allow for interpolating single-station measurements into a continuous map of crustal thickness for the entire study area, providing valuable information for diverse Earth science disciplines from geodynamic modeling to simulation of seismic wave propagation.

2. Tectonic Setting and Previous Geophysical Studies

[5] Northern Morocco is a complex and heterogeneous tectonic setting (Figure 1). Based on the tectonic evolution, it can be divided into three main domains: The Rif chain; the Atlas Domain, an inverted rift that forms an intracontinental active fold-and-thrust belt; and finally, stable zones forming the Moroccan Meseta (the Hercinian Moroccan Massif and Meso-Cenozoic plateaus).

2.1. The Rif Chain

[6] The Rif chain in northern Morocco constitutes the southern branch of the Betic-Rif orogenic belt. It originated

during a Miocene continent-continent collision as a result of about 250 km westward motion of the Alboran domains [e.g., *Platt et al.*, 2003]. The Rif belt is classically divided into three domains according to stratigraphic and tectonic features: the internal and external zones, separated by the Maghrebian Flysch domain. This last domain is formed by sediments originally deposited in an oceanic trough (Maghrebian Trough) and/or a very thin continental crust [*Lujan et al.*, 2006]. The external zones are fold-and-thrust belts of Mesozoic and Tertiary sedimentary rocks deposited in a shelf environment in the Maghrebian passive continental paleomargin. The internal zones constitute the main part of the Alboran domain [*Balanyà and García-Dueñas*, 1987] and are composed mainly of Paleozoic and Mesozoic metasedimentary rocks with varying metamorphic grade, distinguishing three different nappe complexes of continental origin [*Chalouan et al.*, 2001]: the Dorsale Calcaire, the Ghomarides, formed mainly by low-grade metasediments, and the Sebtides with low- to high-grade metamorphic rocks, formed by the accretion of small continental fragments during Eocene time [*Platt et al.*, 2006]. The Ghomarides and Sebtides have their equivalents in the Betic chain in the Malaguides and Alpujarrides. The internal zones of the Rif and the Betic orogen together with the basement of the Alboran basin, formed by the Sebtides-Alpujarrides rocks [*Comas et al.*, 1999], constitute the Alboran domain.

[7] Previous geophysical studies obtained a maximum crustal thickness of 40 km beneath the Rif [*Giese and Jacobshagen*, 1992] although other studies based on gravity, elevation, heat flow, and seismic data suggest a maximum of ~36 km under the Rif mountains, decreasing to a minimum of 30 km toward the coast [*Torne et al.*, 2000; *Fullea et al.*, 2007].

[8] To the southeast, the Rharb (or Gharb) basin separates the Rif chain and the western Morrocan Meseta (see Figure 1). In this basin, the top of the basement is overlain by thrusted and stacked sediments of different age, reaching a maximum depth of 8 km toward the west.

2.2. The Atlas Domain

[9] The Atlas domain is the result of a Mesozoic rifting episode affecting the central North Atlantic and the Western Tethys followed by the Cenozoic collision of the Africa and Iberian plates [e.g., *Jacobshagen et al.*, 1988]. While the Tell Atlas along the Mediterranean coast of eastern Morocco and Algeria has been substantially reworked during plate convergence and the evolution of the western Mediterranean, the NE-SW trending Middle Atlas and E-W trending High Atlas in the interior of Morocco form a domain with different characteristics. In the Atlas, the tectonic shortening is moderate and poorly correlated with topography, suggesting that the crustal root beneath the Atlas Mountains is not deep enough to isostatically support topography reaching up to 4165 m in the High Atlas south of Marrakesh [e.g., *Seber et al.*, 2001; *Teixell et al.*, 2003; *Zeyen et al.*, 2005].

[10] Available geophysical data indicate maximum crustal thicknesses of 38–40 km beneath the most elevated parts of the Atlas [e.g., *Makris et al.*, 1985; *Tadili et al.*, 1986; *Wigger et al.*, 1992; *Fullea et al.*, 2007]. Modeling refraction and wide-angle data, *Tadili et al.* [1986] concluded that crustal thickness varies from 25 km along the Atlantic coast of Morocco to 40 km in the central High Atlas. Later on, *Wigger et al.* [1992] carried out a seismic refraction study of the crustal thicknesses beneath the High Atlas and surrounding area, getting 35–40 km in the Atlas and 30–35 km in the peripheral plain. From receiver function studies, *van der Meijde et al.* [2003] obtained a crustal thickness of 39 km under station MDT (Midelt), located just north of the High Atlas (between TopoIberia stations M018 and M019, see Figure 1). For the same station, *Sandvol et al.* [1998] found two wave speed discontinuities, at 36 and 39 km, and interpreted the shallower one as the crust-mantle boundary.

2.3. The Moroccan Meseta

[11] The High and Middle Atlas mountain belts separate two rigid and stable Paleozoic blocks: the Western Moroccan Meseta and the Eastern Moroccan Meseta. The Moroccan Meseta is an eroded Hercynian belt covered by Mesozoic and Cenozoic series which has remained stable since the middle Paleozoic. Crustal thickness values are scarce for the Moroccan Meseta. Few seismic profiles partially map the Moho discontinuity in this area, obtaining values from 30 to 35 depth [*Wigger et al.*, 1992; *Contrucci et al.*, 2004; *Jaffal et al.*, 2009].

3. Data and Methodology

[12] We calculate *P* wave receiver functions from teleseismic events recorded at 26 seismic broadband stations deployed in the northern part of Morocco (see Figure 1). The largest amount of the data were provided by the temporary TopoIberia experiment (21 stations, blue triangles in Figure 1). Additionally, we analyze five permanent stations: one from the Instituto Andaluz de Geofisica (IAG, station CEUT, red square, http://www.ugr.es/~iag), and four from the Western Mediterranean Network (WM-GE, green squares, stations AVE, IFR, MELI, and PVLZ, http://geofon.gfz-potsdam.de/).

[13] For the receiver function analysis, we consider teleseismic earthquakes with magnitude higher than 5.5 in the distance range between 30° and 90°. Subject to data availability for each station, we analyze between 2 and 4 years of seismicity, which results in a number of usable receiver functions from 32 (ALHU) to 125 (M015). Those extremes reflect mainly different microseismic noise in a coastal setting and at remote inland stations, together with some technical problems for some of the stations. For the study area, the 30° to 90° distance range covers very active seismogenic source areas to the NE (southeastern Asia) and SW (central and south America), while northwestern and southeastern back azimuths are less represented.

3.1. Receiver Function Analysis

[14] The *P* wave receiver functions are time series containing *Ps*-converted and multiply reverberated phases generated at seismic discontinuities beneath the recording stations [*Vinnik*, 1977; *Langston*, 1979]. Teleseismic *P* receiver functions are obtained by deconvolving the vertical component from the horizontal components in the time window corresponding to the first *P* arrival and its coda. Ideally, the deconvolution process completely removes the signature of the source time function, source-side path effects, and the instrument response from the waveforms,

retaining just the information on receiver-side wave conversion caused by the local structure beneath the seismic station [*Langston*, 1979].

[15] Receiver functions have been obtained using an iterative time domain deconvolution method [*Ligorria and Ammon*, 1999]. The time domain approach consists of approximating the deconvolution response through a series of Gaussian pulses with adjusted amplitudes and time lags. This technique circumvents stability problems intrinsic to spectral division, leads to a causal response, and generally produces more stable results in the presence of noise [*Ligorria and Ammon*, 1999]. We use a Gaussian filter width of 2.5, translating into receiver function pulses around 1 s wide. The time windows used are 120 s long, starting 20 s before the *P* arrival. We only calculate the receiver functions for earthquakes with a signal-to-noise ratio larger that 2.

[16] Prior to deconvolution, we decimate the seismograms to 10 samples per second and filter them with a Butterworth bandpass filter from 20 s to 5 Hz. Then we rotate the horizontal and vertical components into the ray coordinate system, using the theoretical incident angle computed in an IASP91 Earth model, thereby obtaining the *Q* and *L* components instead of radial and vertical components, respectively [*Vinnik*, 1977]. This rotation eliminates in the *Q* component the energy of the direct *P* present in the radial component, allowing a better observation of shallow crustal discontinuities and sedimentary layers [*Vinnik*, 1977]. In the case of a laterally homogenous and isotropic medium the *P*-to-*S* conversions should only be recorded in the *Q* component, while the transversal component of the *P* receiver function is predicted to be identical to zero. Energy in the transverse component is explained by lateral heterogeneity of the medium, in particular by dipping layers, or anisotropy [e.g., *Cassidy*, 1992]. We examine both *Q* and *T* components, and their variations in back azimuth, to check for heterogeneity and to help the interpretation of complex receiver functions.

[17] We evaluate receiver function quality by convolving them with the *L* component of the signal and checking how well this convolution reproduces the original *Q* and *T* components of the seismograms. We keep only the receiver function that can reproduce 80% of the original signal.

3.2. Data Examples

[18] To illustrate some characteristics of northern Morocco receiver functions, we show examples of some representative stations in Figures 2 and 3.

[19] We display the receiver functions in two ways. First, we show the *Q* and *T* components of all the receiver functions sorted by back azimuth and corrected by *Ppps* moveout, along with the back azimuth of each trace (named baz in Figures 2 and 3). The aim of the moveout correction is to equalize differences in ray parameters in the phase arrival times to allow for direct comparison of receiver functions for earthquakes from different distances. We choose to perform a *Ppps* moveout correction instead of *Ps* moveout in order to enhance the multiples in the summation traces only for visual purpose. With this moveout, the arrival time of the Moho conversion phase, *Ps*, is not appreciably misplaced in the summation traces. We use a ray parameter of 0.065 s km^{-1} (slowness of 7.0° s^{-1}) as reference. This representation gives us information about laterally varying structures and the complexity of the discontinuities (e.g., the presence of dipping, scattering and/or anisotropy [e.g., *Cassidy*, 1992; *Jones and Phinney*, 1998]. In addition, we show the *Q* receiver functions stacked and sorted by the ray parameter (Figures 2, right, and 3, right). We stacked them into bins of 0.03 s km^{-1}, moving the bin every 0.01 s km^{-1}. This representation helps us to distinguish between converted and multiple phases. The converted phases exhibit a positive moveout with respect to the direct *P* with increasing ray parameter, while the multiples present a negative moveout.

[20] Figure 2 displays three stations along a north-south profile, probing the structure of the internal (NKM) and external zones (M012) and the Morrocan Meseta (M017). Station NKM, located in the Gibraltar arc near the boundary between the internal and external zones, shows great intracrustal complexity and relevant signal in the transverse component of the receiver functions. The change of polarities in the *Q* component (and less clear in *T*) at ~3 s indicates a dipping structure and/or some anisotropy at the intracrustal level. Despite complexity at NKM, the Moho conversion (after 5.4 s) can be identified as the largest pulse in the *Q* receiver function, and also the first Moho multiple is clear (*PpPms* at ~17.6 s). The conversion phase is missing in the restricted back azimuth range of [180°–270°]. To confirm that those phases are the converted and the multiple, in Figure 2 (right) we plot stacked receiver functions sorted by the ray parameter. The dashed red lines mark the theoretical arrival times with the ray parameter for the converted phase and the multiples. As we can observe, the selected converted phase follows a positive moveout with increasing ray parameter, and the first multiple follows a negative moveout.

[21] Station M012 also shows an intracrustal discontinuity, but the traces appear less complex and the energy in the *T* component is lower than in the case of station NKM, indicating near horizontal intracrustal and Moho discontinuities. The Moho conversion has a delay time similar to that for NKM, indicating that there is also a thick crust beneath the external zones of the Rif chain. At station M017 in the foreland, receiver functions show less signature of crustal structure. The Moho conversion and multiples are clear, indicating a much shallower Moho (*Ps* at 3.8 s) compared to NKM and M012 (*Ps* at 5.4 and 5.1 s, respectively).

[22] Figure 3 displays three stations along a southwest-northeast profile from the Middle Atlas (stations M018 and M014) to station TAF near the Algerian border and Mediterranean coast. At M018, the Moho conversion at 3.7 s, and multiples indicate similar crustal thickness as below M017. Station M014 shows remarkably different receiver functions, although it is located in the same geologic domain (Atlas domain) and is only 70 km from station M018. Receiver functions at M014 are very simple and show little energy in the *T* component. The Moho conversion and its multiples are clear, indicating a much shallower Moho, with the *Ps* conversion arriving after 3.3 s (*Ps* at 3.8 s in M018). At station TAF there is a strong conversion from a shallow crustal discontinuity, but otherwise receiver functions are very similar to M014 despite the large distance between the stations, with low energy in the *T* component and the Moho conversion, *Ps*, at 3.2 s.

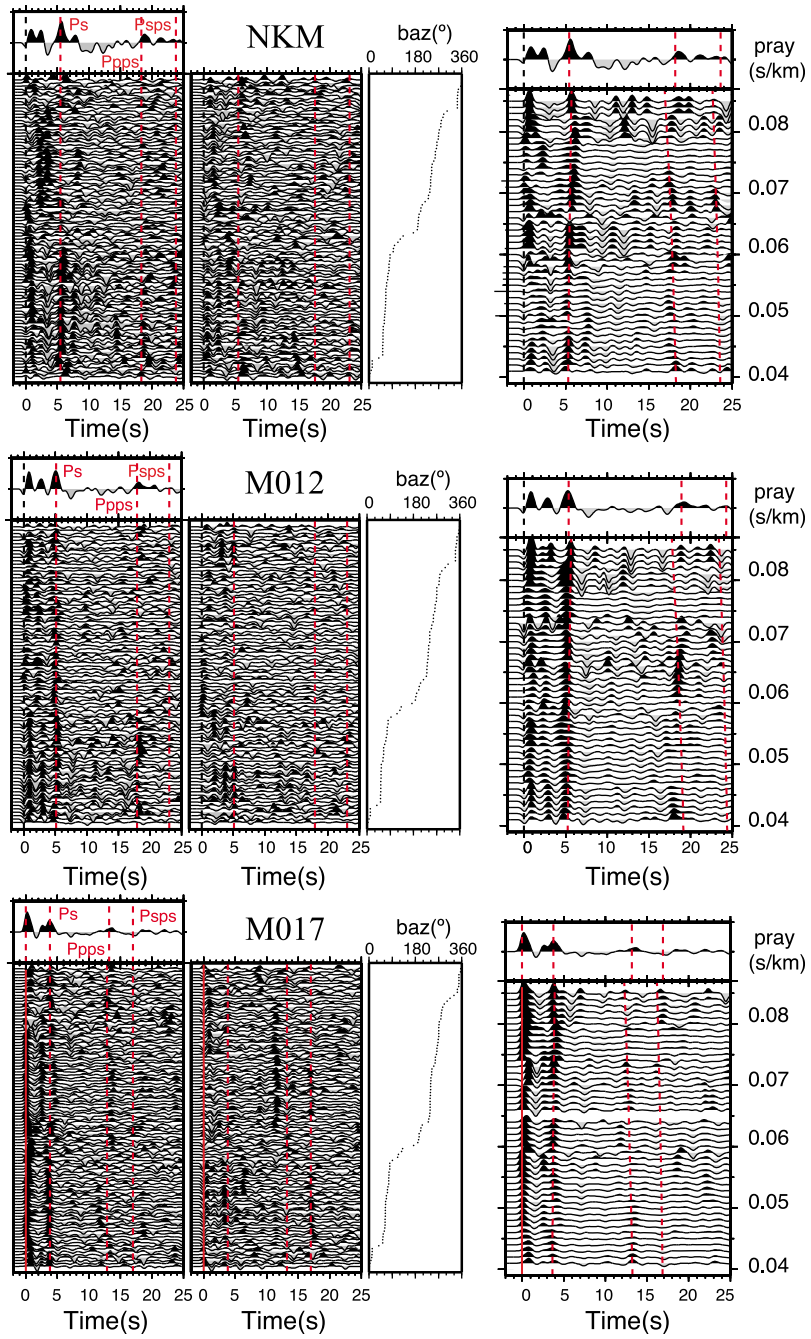

Figure 2. Receiver functions along a north-south profile in northwestern Morocco, including stations NKM, M012, and M017. (left) Plot of the *Q* and *T* components of the receiver functions, sorted by back azimuth and corrected by *Ppps* moveout, along with a plot of the back azimuth of each trace. At the top, the summation trace of the *Q* components of the receiver functions is displayed. (right) The *Q* receiver functions stacked and sorted by the ray parameter (noted pray). We stacked them into bins of 0.03 s km^{-1} moving the bin every 0.01 s km^{-1}. The dashed red lines mark the theoretical arrival times for the converted (*Ps*) and the multiple phases (*Ppps* and *Psps*) at the Moho discontinuity for the crustal thickness and V_p/V_s ratio obtained in this study.

3.3. Crustal Thickness Calculation

[23] To calculate the crustal thickness, we use the relative traveltimes for the converted phase at this discontinuity, *Pms*, and its multiples, *PpPms* and *PpSms* + *PsPms* phases, with respect to the direct *P* arrival. These relative traveltimes can be employed to constrain the thickness (H) and V_p/V_s ratio of the crust, provided that the average *P* wave speed is known [*Zandt and Ammon*, 1995]. We apply a receiver function stacking technique developed by *Zhu and Kanamori* [2000], involving a grid search in the H and V_p/V_s space. We use steps of 0.1 km and 0.01, respectively. In this

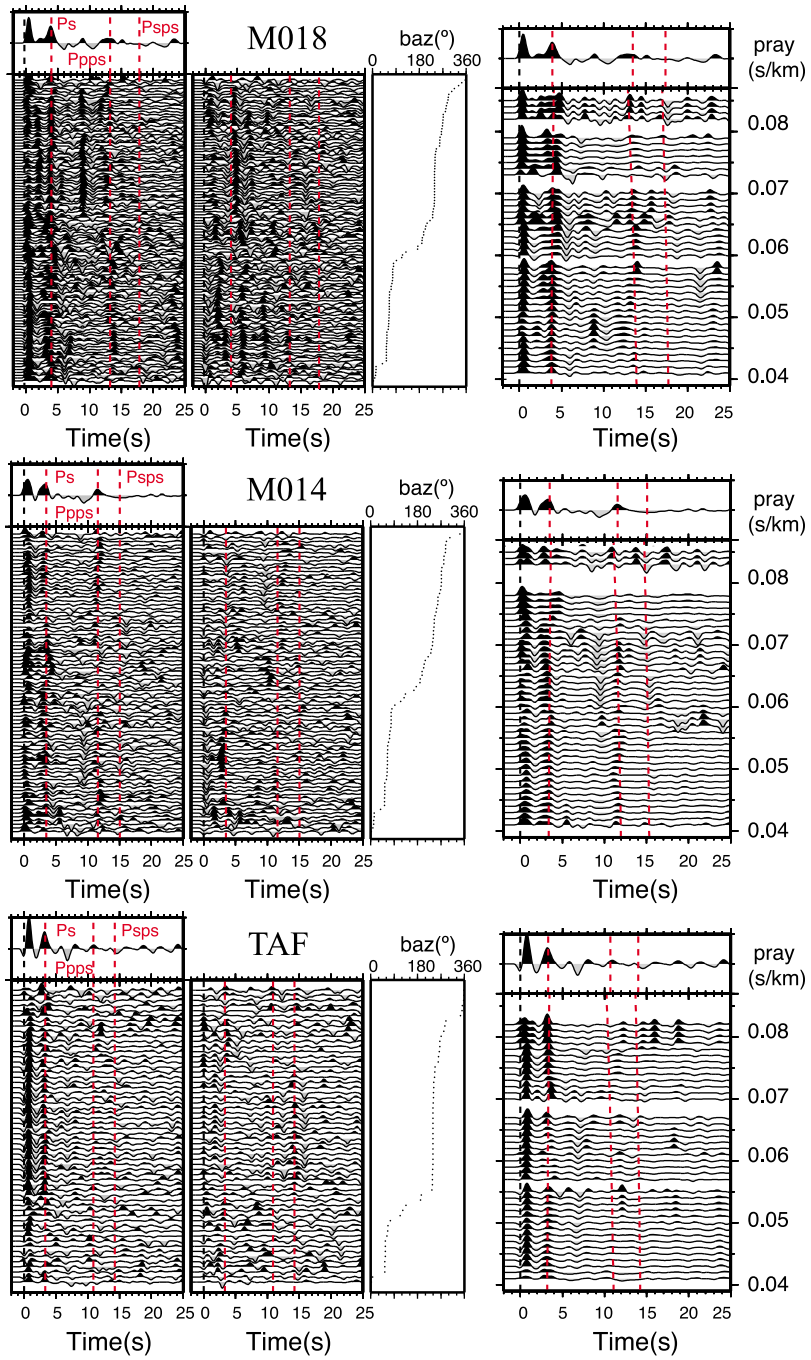

Figure 3. Same as Figure 2 but for receiver functions along a southwest-northeast profile from the Middle Atlas to northeastern Morocco, including stations M018, M014, and TAF.

approach, coherent phases are constructively superposed, while noncoherent signals tend to be eliminated if the number of records is large enough. The location of the maximum in the stacking surface, therefore, provides the estimates for H and V_p/V_s. To estimate the uncertainties, we used a bootstrap approach [*Efron and Tibshirani*, 1991]. We base our statistics on 200 bootstrap replications which means we repeat the stacking procedure 200 times with a resampled data set selected randomly from the original data set. The sampled set has the same size as the original but may contain duplicates of receiver functions. The covariance matrix is then obtained by applying the standard formulae for the mean, variance, and covariance to the bootstrap estimates. For some stations, the stacking surfaces (normalized to 100%) are shown in Figure 4 along with the 1σ confidence ellipses (red) from the bootstrap analysis. The average V_p used in the grid search was obtained from previous refraction profiles in the area, 6.3 km s^{-1} for the internal and external zones [e.g., *Banda et al.*, 1993; *Fernández et al.*, 2004] and 6.2 km s^{-1} in the Atlas and the Moroccan Massif [*Tadili et al.*, 1986; *Wigger et al.*, 1992]. Plausible deviations from those average values (e.g., 0.25 km s^{-1})

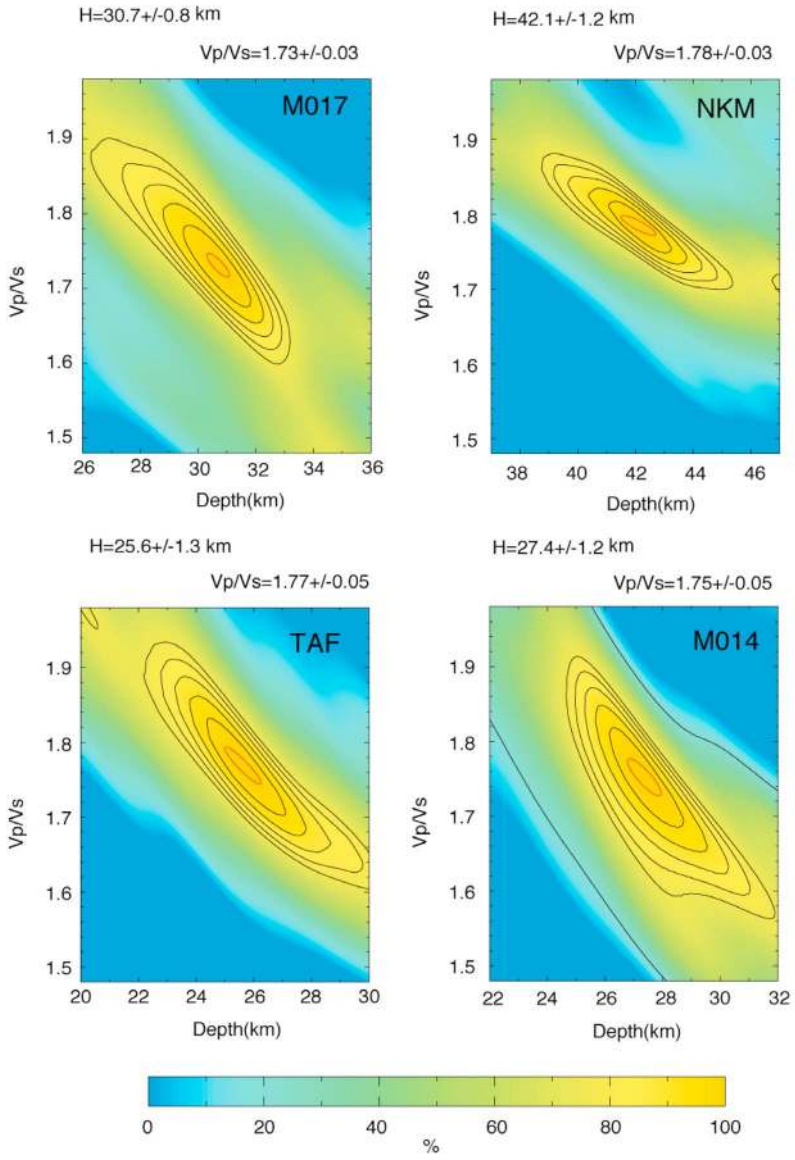

Figure 4. Examples of the grid search analysis to obtain the crustal thickness and the V_p/V_s ratio using the *Zhu and Kanamori* [2000] method. The values are displayed in Table 1. The stacking surfaces (normalized to 100%) are shown along with the 1σ confidence ellipses (red ellipse).

lead to relatively minor (e.g., 1 km) bias in depth for typical crustal thickness values.

[24] This receiver function stacking method has limitations in the presence of a dipping Moho, a gradient-type crust-mantle boundary instead of a sharp, well-defined Moho discontinuity, or in sedimentary environments, where the multiples from the sediment-bedrock interface may overlap with the *Ps*-converted phase at the Moho [e.g., *Julià et al.*, 2003]. For the stations for which the above methodology is not applicable due to a lack of clear multiples or weak Moho conversions, the grid search maxima are poorly constrained or indicate implausible values due to the superposition of unrelated phases. In those cases, we estimate the crustal thickness by picking the *Ps* arrival in the summation trace after applying a *Ps* moveout correction. We associate the Moho conversion with the last clear pulse of the initial pulse train in the receiver functions. We convert delay time to depth using the average V_p/V_s ratio from receiver function, stacking results at the rest of the stations belonging to the same domain and the average V_p wave speed from previous geophysical studies.

[25] To illustrate the accuracy of this option when dipping layers are present, we have performed a test with synthetic receiver functions for a 30 km dipping crust with an average V_p/V_s = 1.73 over a half-space using the *Frederiksen and Bostok* [2000] code, which allows the inclusion of dipping layers in 1-D Earth models. Our test consists of a 30 km thick layer over a half-space with dipping angles of 0°, 5°, 10°, 15°, and 20°. The receiver functions have been computed for waveforms approaching the structure from a full range of back azimuths (0°–360°) for the reference ray parameter (0.065 s km^{-1}), and we obtain the summation

Table 1. Estimates for Crustal Thickness and V_p/V_s Ratio[a]

Station	Quality	N_RF	Baz (deg)	Tps (s)	V_p^{ave} (km s^{-1})	V_p/V_s^{ave}	H^{Ps} (km)	H^{zhu} (km)	V_p/V_s^{zhu}	Corr. (%)
ALHU	c	32	all	3.1	6.3	1.75	24.7			
AVE	b	50	all	4.1				32.2 ± 1.9	1.77 ± 0.04	−0.98
CEUT	b	124	all	5.1				40.1 ± 1.2	1.77 ± 0.02	−0.97
CHAF	b	51	all	2.6				23.0 ± 1.9	1.69 ± 0.07	−0.80
IFR	a	111	all	3.5				32.2 ± 0.5	1.66 ± 0.02	−0.83
M001	a	48	all	4.1				32.8 ± 0.4	1.75 ± 0.02	−0.90
M002	b	86 (54)	[180–360]	4.5				37.7 ± 0.8	1.73 ± 0.03	−0.96
M004	b	50	all	4.6				37.6 ± 1.0	1.75 ± 0.05	−90
M005	b	64 (32)	[180–280]	5.0				39.6 ± 1.2	1.77 ± 0.05	−0.97
M006[b]	b	90	all	5.2 [6.4]	6.3	1.75	41.5 [51.1]			
M007	c	63	all	3.3	6.3	1.75	26.3			
M008	c	97	all	3.4	6.2	1.71	29.9			
M010	a	80	all	4.6				33.5± 2.2	1.81 ± 0.06	−0.98
M011	c	83	all	4.0	6.2	1.75	31.5			
M012	a	88	all	5.1				44.4 ± 2.4	1.72 ± 0.04	−0.94
M013[b]	b	53	all	3.4 [6.3]	6.3	1.75	27.2 [50.3]			
M014	a	81	all	3.3				27.4 ± 1.2	1.75 ± 0.05	−0.80
M015	b	125 (52)	[0–180]	4.2				34.4 ± 0.3	1.68 ± 0.02	−0.87
M016	b	57 (36)	[0–90] & [270–360]	4.2				32.8 ± 1.0	1.77 ± 0.4	−0.93
M017	a	102	all	3.8				30.7 ± 0.8	1.73 ± 0.03	−0.84
M018	b	106 (46)	[0–180]	3.9				32.4 ± 1.8	1.71 ± 0.06	−0.97
M019	c	93	all	3.4	6.2	1.75 [1.66]	26.8 [∼31]			
MELI	c	87	all	2.7	6.3	1.75	21.6			
NKM	b	96	all	5.4				42.1 ± 1.2	1.78 ± 0.03	−0.87
PVLZ[b]	c	68	all	4.4 [6.5]	6.3	1.75	35.1 [52.0]			
TAF	b	58	all	3.2				25.6 ± 1.3	1.77 ± 0.05	−0.93

[a]Quality a distinguishes clear multiples in receiver functions, quality b distinguishes some good back azimuth, and quality c distinguishes no clear multiples. N_RF and Baz indicate the total number of receiver functions and whether all back azimuths or a selected range were used for stacking (in this case the number in brackets is the corresponding number of receiver functions). Tps is the arrival time of the *Ps* conversion. H^{Ps} denotes crustal thickness for stations where $H - V_p/V_s$ grid search could not be applied, and H_p^{ave} and V_p/V_s^{ave} denote the average parameters for the corresponding tectonic domain that were applied to convert Ps delay times to crustal thickness. Grid search results for H^{Zhu}, and V_p/V_s^{Zhu} are given with their error estimates from bootstrap analysis and correlation (Corr.).

[b]For stations PVLZ, M006, and M013, the values in brackets refer to last clear *Ps* conversion in the traces, interpreted to represent a subcrustal discontinuity in these cases.

traces. The difference in the arrival time of the converted phase at the Moho discontinuity in the summation traces between a horizontal Moho and a 20° dipping Moho is ∼0.2 s, corresponding to an underestimation of 1.6 km in crustal thickness. Applying this ideal back azimuth distribution to the *Zhu and Kanamori* [2000] method results in 26.3 km of crustal thickness (underestimation of 3.7 km) and a V_p/V_s of 1.82 (overestimation of 0.09). In general, the application of this Zhu and Kanamori method to dipping structure leads to an underestimation of the Moho depth and an overestimation of the V_p/V_s ratio (see *Lombardi et al.* [2008] for a discussion about Zhu and Kanamori method and dipping Moho).

[26] The vertical resolution of the receiver functions is controlled by the wavelength of the *Ps*-converted phase, which depends on the spectral content of the recorded signal and the velocity of the medium. Material property gradients occurring over a depth range of a half wavelength can be identified and well characterized. Average *S* wavelengths are 3.5 and 4.5 km in the crust and upper mantle, respectively, for a 1.0 s dominant period. This means that the minimum thickness resolvable for discrete homogeneous layers is ∼2 km in our case.

[27] Some of the receiver functions in this study present significant energy in the transverse components (see Figures 2 and 3). In the case of NKM, M018, and M017, the two approaches produce similar crustal thickness values, implying moderate dipping under the stations. For example, NKM H^{Ps} = 43.1 km and H^{Zhu} = 40.1, M018 H^{Ps} = 32.3 km and H^{Zhu} = 32.4 km, and M017 H^{Ps} = 29.9 km and H^{Zhu} = 30.7 km. This difference increases when amplitude size in the transverse as expected (e.g., NKM). For these stations, our approach has been to report the results of the *Zhu and Kanamori* [2000] method in Table 1.

4. Results

[28] From analyzing 2–4 years of global seismicity, we were able to obtain more than 2000 usable receiver functions altogether, giving an average of about 80 receiver functions for each of the 26 recording stations deployed over northern Morocco. As already illustrated through the data examples in Figures 2 and 3, receiver functions indicate significant regional and local variations of lithospheric structure. The delay times of the Moho conversions range from 2.7 s at station MELI to 5.4 s at station NKM, corresponding to a factor of ∼2 in crustal thickness. Receiver functions for individual stations may be very simple (e.g., M014), but frequently they evidence local complexity beneath the recording stations, manifested in strong intracrustal conversions and relevant signal in the transverse receiver functions (e.g., NKM). Although some back azimuths are underrepresented due to the characteristics of global seismicity, the available traces usually allow tracking the Moho conversion over a broad azimutal range. Sometimes slight timing variations in the *Q* component and polarity changes in the *T* component indicate local dip of the Moho interface beneath

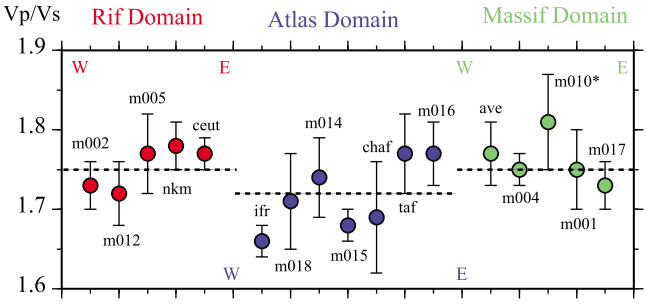

Figure 5. Estimates for the ratio (V_p/V_s^{Zhu} obtained from receiver function stacking and $H - V_p/V_s$ grid search, grouped according to the corresponding tectonic domains. Inside each domain, they are ordered geographically from west to east. In the Alboran domain and the foreland, normal average values around 1.75 were obtained, while the Atlas domain shows a lower average V_p/V_s^{Zhu} ratio of 1.71.

the stations. We report average values for crustal thickness in this study.

[29] Most stations, 17 altogether, show sufficiently clear Moho conversions and *PpPms*, *PpSms* + *PsPms* multiples to apply the receiver function stacking technique described in section 3 and to provide well-constrained estimates for H and V_p/V_s through the grid search approach (compare examples in Figure 4). The obtained values for crustal thickness (noted by H^{Zhu}) and V_p/V_s ratio (V_p/V_s^{Zhu}) along with 2σ confident bounds and the correlation factors are summarized in Table 1. The crustal thicknesses are well constrained with uncertainties ranging from 0.4 to 2.8 km and the V_p/V_s ratios varying from 0.02 to 0.07. In all our results, the correlation coefficients in Table 1 (the covariance matrix cross term) exhibit large and negative values. This means that even though the usage of the arrival times of three different phases in the stacking technique reduces the trade-off degeneracy in the determination of H and V_p/V_s [*Zhu and Kanamori*, 2000], this trade-off is still present with different degrees in our analysis. The large correlations imply that the estimated values for V_p/V_s and H do not vary independently within the uncertainty limits.

[30] Crustal thickness variations are discussed in detail in section 5. The average V_p/V_s ratios show normal values of ~1.75 for most stations. Bootstrap-based error bounds for H^{Zhu} and V_p/V_s^{Zhu} are reported in Table 1. Some more insight can be gained by grouping V_p/V_s ratio estimates by tectonic domain (Figure 5). In the Rif chain and foreland, only minor variations around an average ratio of 1.75 are observed, with the exception of a large V_p/V_s ratio of 1.81 at station M010, attributed to the sedimentary cover in the Rharb foreland basin. Cases of anomalous low V_p/V_s ratios are limited to the Atlas domain, where the average values are around 1.71. The minimum V_p/V_s ratio is 1.66, corresponding to a well-constrained grid search minimum for station IFR. The low values and their high variability within the domain suggest the influence of an irregular distribution of felsic rocks in the Atlas crust [*Christensen*, 1996; *Wigger et al.*, 1992]. Generally, the consistent and plausible values obtained for V_p/V_s^{Zhu} suggest that estimates of H^{Zhu} show little bias due to the problematic trade-off between both parameters and support reliability of inferred crustal thickness values within their statistical errors.

[31] For nine stations altogether where the H and V_p/V_s grid search led to unstable results, we convert the *Ps* delay times to crustal thicknesses (H^{Ps} in Table 1) using the average V_p/V_s^{ave} ratio of the corresponding tectonic domain (Figure 5) and average V_p wave speed V_p^{ave} of 6.3 km s^{-1} for the Rif [e.g., *Banda et al.*, 1993; *Fernández et al.*, 2004] and 6.2 km s^{-1} in the Atlas and the Moroccan Massif [*Tadili et al.*, 1986; *Wigger et al.*, 1992].

[32] An example of problematic stations is M013; receiver functions are shown in Figure 6. The identification of the

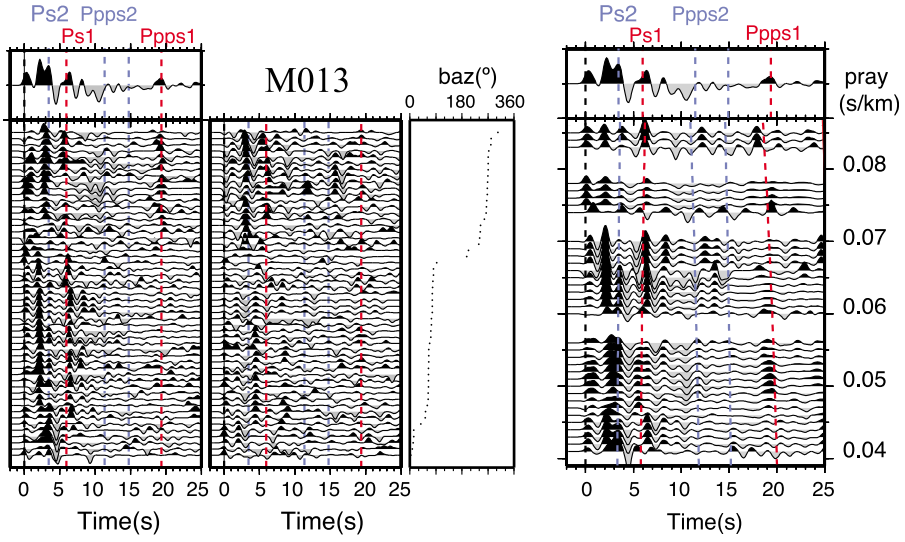

Figure 6. Same as Figure 2 but for receiver functions obtained at station M013. In this case, identification of the *Ps* conversion and their multiples is problematic. We highlight the penultimate (*Ps*2, blue lines) and last (*Ps*1, red lines) pulses of the initial pulse train as possible Moho conversions. *Ps*2 is our preferred interpretation, taking into account receiver functions at neighboring stations as well as the particular geodynamic setting of this station (see text).

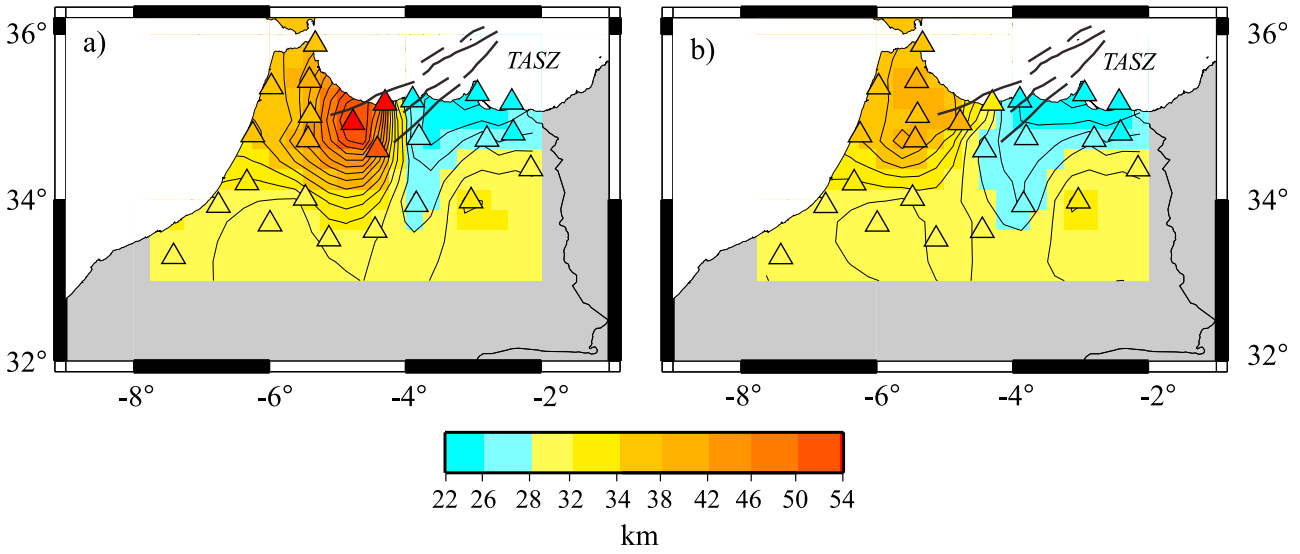

Figure 7. Stations (triangles) color coded according to crustal thickness and interpolated Moho surface for northern Morocco. Large variations, strong gradients, and a division into three different domains are observed (light blue, yellow, and orange, respectively). Two alternative interpretations for stations in the central Rif are provided, picking the (a) later or (b) earlier of two possible Moho conversions (see receiver functions in Figure 6). We prefer interpretation in Figure 7b for the Moho and attribute the apparent indentation in Figure 7a to the presence of a subcrustal discontinuity in this sector (see text). Thick black lines mark the position of the main faults of the trans-Alboran shear zone (TASZ).

pulse corresponding to the Moho conversion is unclear as two pulses of similar amplitude are present within the time range of possible Moho conversions and have positive moveout with increasing ray parameter (*Ps*1 and *Ps*2 in Figure 6). Regarding its multiples, a possible first multiple is observed at 19.1 s but only for some back azimuths (*Ppps*1, see Figure 6). This phase presents a negative moveout with increasing ray parameter, supporting that it is a multiple. For this station, the receiver function stacking technique does not provide a stable solution. Similar features are found at two neighboring stations, PVLZ and M006, also located in the Rif mountain belt (see Figure 1), with the identification of two possible Moho conversion pulses and a *PpPms* multiple at ~19.4 s. Two alternatives have been considered for these stations. Our usual strategy of associating the Moho conversion with the last converted phase of the initial pulse train in the receiver functions (*Ps*1 in Figure 6 for station M013) leads to very large crustal thicknesses (50–52 km, see Table 1) compared to nearby stations, e.g., ALHU and M007 (crustal thicknesses of ~25–26 km, Table 1 and Figure 1). The delay times of the last pulse for stations M013, PVLZ, and M006 range between 6.3 and 6.5 s, while for stations ALHU and M007 the delay times are 3.1 and 3.3 s, respectively.

[33] Alternatively, we prefer associating the Moho conversion pulse with the penultimate pulses of the initial pulse train (*Ps*2; for M013 in Figure 6) and attribute the last pulse to a subcrustal discontinuity (*Ps*1, Figure 6). The observed delay times of *Ps*2 for stations M013, PVLZ, and M006 are 3.4, 4.4, and 5.2 s, respectively, corresponding to crustal thicknesses of ~27, ~35, and ~42 km. For this last interpretation, the Moho discontinuity is shallower, and the transition to the surrounding stations is smoother.

[34] Presenting our estimates of crustal thickness in a map (Figure 7), a consistent regional pattern emerges albeit with the complexity manifested in receiver functions from individual stations and the lateral heterogeneity inferred from comparing nearby stations. We color code individual thickness measurements in each station symbol and interpolate single-station measurements into a continuous map of crustal thicknesses for the entire study area. A continuous curvature gridding algorithm (GMT software [*Wessel and Smith*, 1998]) has been used for interpolation. To reduce oscillation of the interpolation surface outside the station coverage, the crustal thickness along the southern limit has been fixed to 32 km.

[35] The most fundamental characteristics of the Moho beneath northern Morocco are the large variations of the crustal thickness (between 22 and 44 km), the presence of strong lateral gradients (most notably near the eastern termination of the Rif mountain chain), and a clear geographic division into three regions with different properties: Large crustal thicknesses are found for entire northwestern Morocco (Rif domain, crustal thicknesses ~35–44 km), northeastern Morocco is affected by significant crustal thinning (crustal thicknesses ~22–30 km), and the foreland farther south shows intermediate crustal thicknesses close to the average values for continental crust (crustal thicknesses ~31 km).

[36] Station M019 is placed in the anti-Atlas region. The closest station to M019 is located 185 km away (station M018), on the other side of the Atlas belt (see Figure 1). Because of its separation from the other stations, its average crustal thickness is not included in the crustal thickness map (Figure 7). This station presents a Moho converted phase at 3.4 s (Table 1) and no clear multiples. If we translate into depth the arrival time of the converted phase using the average V_p/V_s ratio for the massif domain (1.75, Figure 5), its crustal thickness is 26.8 km. This value represents a surprisingly thin crust, considering that it is located on the

edge of a craton. From a refraction profile, the crustal thickness estimations for the area is ~34 km [*Wigger et al.*, 1992]. On the other hand, its receiver functions have a lot of similarities with the ones at station IFR with an V_p/V_s ratio from the *Zhu and Kanamori* [2000] method analysis of 1.66. Using the low V_p/V_s ratio of station IFR, we get a crustal thickness for M019 of ~31 km. This values is similar to the ones obtained for the stations located in the massif domain (e.g., AVE and M017) but with a lower V_p/V_s.

5. Discussion

[37] We provide two alternative interpretations for three neighboring stations (PVLZ, M006, and M013) in the central sector of the Rif mountain belt (Figures 7a and 7b). As we discuss above, these receiver functions show, after some initial intracrustal signal, two pulses of similar amplitude within the time range of possible Moho conversions. These pulses have some overlap for M006 and are separated for M013 and PVLZ. For PVLZ, M006, and M013, associating the Moho with the last clear pulse of the initial pulse train leads to depths of 50–52 km (Table 1) and to a strong indentation of the interpolated Moho interface around these stations (see Figure 7a). We prefer associating the Moho with the earlier pulse in this case, leading to a shallower Moho and a smoother transition toward the surrounding stations. Supporting this interpretation, we found that at station M012 (compare Figure 2) there is no evidence for large dips, as would be expected under the first hypothesis, nor is there evidence for large dips close to ~25° between stations M013 and M007 (Figure 6) or to ~30° between PVLZ and ALHU at only ~37 km distance. Therefore, the later pulse is inferred to be the signature of a subcrustal discontinuity. The locations of stations PVLZ, M006, and M013 coincide with a domain of anomalous GPS velocities inside the Rif [*Fadil et al.*, 2006; *Tahayt et al.*, 2008] that can be modeled by a small patch of basal traction in this area [*Pérouse et al.*, 2010] thought to represent delamination and rollback of the lithospheric mantle [e.g., *Seber et al.*, 1996; *Faccenna et al.*, 2004]. We associate the second pulse with such subcrustal structure. A detailed interpretation of this presumed mantle conversion is beyond the scope of this paper and the methodology applied.

[38] The entire area of northwestern Morocco is underlain by a thickened crust, showing thicknesses of 35–44 km from the Gibraltar Strait to the north to about 34.5°N latitude to the south and from the Atlantic coast to about 4.5°W longitude. A deep Moho can be found under all units of the Rif in this sector: internal zones, flysch units, and external zones. Farther east, a zone of very relevant crustal thinning extends all the way to the Algerian border, between the Mediterranean coast and about 34.5°N latitude. In this sector, crustal thicknesses range from 22 to 30 km. The crustal thickness is increasing from the coast (ALHU, MELI, CHAF, 22–25 km) to the south (M013, M014, M008, 27–30 km), with station M014 providing evidence for some continuity of this domain into the Middle Atlas, where the transition to normal crustal thickness values is located between stations M014 and M018 (compare Figure 3). The sharp contrast between thinned and thickened crust, located at about 4°W at the coast (~35 km at PVLZ and ~25 km at ALHU) and 4.5°W farther inland (42 km at M006 and 27 km at M013) is remarkable. No intermediate crustal thickness, indicating a transition, has been observed at this station deployment, with the possible exception of station PVLZ. Plotting individual thickness measurements onto a roughly west-east oriented profile across the thickened and thinned domains illustrates the amount of thinning, the sharpness of the transition, and its spatial coincidence with the subcrustal discontinuity (Figure 8a).

[39] This abrupt change of crustal thickness of ~10–15 km crosscuts at least the external zones and possibly all units of the Rif. This suggests that the formation of this major lithospheric heterogeneity, or alternatively the propagation to the current position, postdates the main orogenic phase in the Rif and is rather related to extensional processes that have affected the Alboran basin since the Miocene. The position of this heterogeneity coincides with the trans-Alboran shear zone, a large, left-lateral transcurrent fault system extending from southeastern Spain across the Alboran Sea into the Rif [*de Larouzière*, 1988]. The trans-Alboran shear zone is believed to play an important role in regional tectonics, accumulating currently ~2 mm yr^{-1} of slip [*Stich et al.*, 2006]. The deepening of the Moho is also correlated with (1) a transition from high heat flows to the east (~80–100 mW m^{-1}) to lower values to the west (~40–60 mW m^{-1} [*Rimi et al.*, 1998; *Pollack et al.*, 1993]), (2) the occurrence of middle Miocene to Pleistocene volcanism, cropping out in a roughly NE-SW trending band extending from southeastern Spain into northeastern Morocco [*Duggen et al.*, 2004], (3) a change in the geoid and Bouguer gravity anomalies from positive to the east to negative to the west (from EGM2008 Global model [see *Fullea et al.*, 2010; *Hildenbrand et al.*, 1988]), and (4) an abrupt change in anisotropic parameters [*Diaz et al.*, 2010]. In addition, as we have discussed before, this area features basal traction indicative of subcrustal tectonic processes (GPS measurements [*Fadil et al.*, 2006; *Tahayt et al.*, 2008]). The east-west change of crustal thickness appears to fit within a general picture of slab rollback and detachment in the westernmost Mediterranean [*Faccenna et al.*, 2004], with a slab tear located near stations PVLZ and ALHU and significant crustal thinning to the east. Particularly remarkable is an apparent extension of the northeast Moroccan thinned crust under the rim of the Middle Atlas belt (station M014, see Figure 1).

[40] Farther south, in the Atlas domain and the Moroccan foreland, crustal thickness shows less variation and average values around 32–33 km (Figures 7 and 8b). Such a crustal thickness is in contradiction to isostatic compensation of the crust. Although the station deployment does not cover the highest altitudes, it includes several stations farther east (stations IFR, M018, and M019) in close proximity to the main chain and topography exceeding 3000 m. Our study is consistent with the hypothesis of a lack of a crustal root beneath the Atlas chain, which is a long debated problem [e.g., *Teixell et al.*, 2005; *Zeyen et al.*, 2005; *Missenard et al.*, 2006]. This apparent lack of isostatic compensation has been attributed to an anomalous depth of the lithosphere-asthenosphere boundary [e.g., *Seber et al.*, 1996; *Teixell et al.*, 2005; *Fullea et al.*, 2010]. The hot, low-velocity mantle underneath the Atlas seems to support the topography [e.g., *Seber et al.*, 1996; *Fullea et al.*, 2010]. From our study we cannot exclude the presence of a crustal root that could provide isostasy for

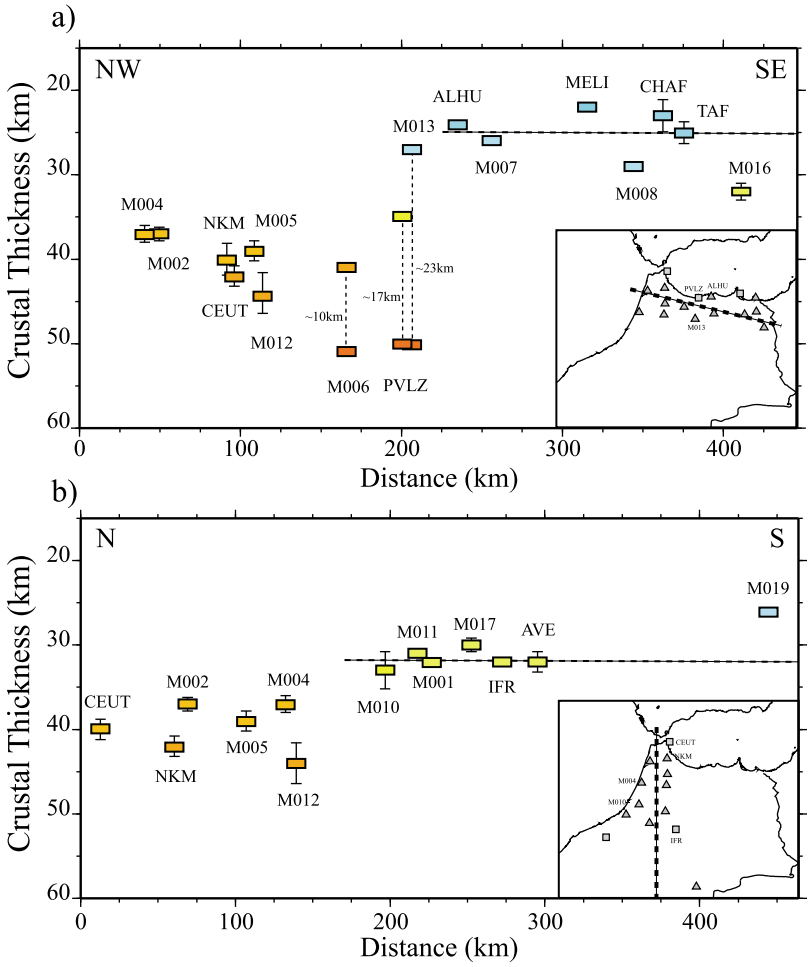

Figure 8. Two profiles showing crustal thickness variations in the study area. (a) The approximately NW-SE profile cuts the transition between the thickened and thinned crust regions, and (b) the N-S profile probes the Rif chain and the Moroccan Meseta. In Figure 8a, at PVLZ, M006, and M013 the depths of the Moho and the subcrustal discontinuity are displayed. The color is in agreement with the color code used in Figure 7.

the central High Atlas, but we can restrict the extension of such structure and confirm that high topography adjacent to the main chain seems to not be compensated for at the crustal level.

[41] Several gaps in the station deployment (e.g., northeast of stations M010, IFR, and M014, respectively) do not exceed 100 km and coincide with areas where the surrounding stations give a relatively consistent picture. On the other hand, for the Atlas and foreland domains the coverage is still sparse, and future studies will have to test the hypothesis of lateral homogeneity emerging from our data. In the meantime, the crustal thickness measurements reported in this study indicate the presence of three fundamentally different domains reflecting different geodynamic evolutions.

6. Conclusions

[42] The crustal thickness map inferred from wave conversions beneath 26 temporary and permanent broadband stations in northern Morocco leads to a fairly complete image of the crust-mantle boundary over the entire region. The present study shows three regions each with rather homogeneous characteristics. All of northwestern Morocco is underlain by a thickened crust (crustal thicknesses ~35–44 km), and northeastern Morocco is affected by significant crustal thinning (crustal thicknesses ~22–30 km). The presence of a subcrustal discontinuity near the border between these two regions has been inferred. Particularly remarkable is an apparent extension of the northeast Moroccan thinned crust under the rim of the Middle Atlas belt. Farther south, an extended region with an average 32 km crustal thickness is found covering not only the Marrocan Meseta but also some areas of the Middle Atlas domain. This seems to support that high topography on the stations located in the Middle Atlas domain is not isostatically compensated for at the crustal level. The obtained V_p/V_s values have minor variations around an average of 1.75 for stations located in the Rif and the foreland units. Anomalously low V_p/V_s values are limited to the Atlas domain, hosting felsic rocks.

[43] This contribution benefits from a high-density coverage of broadband seismic stations beneath northern Morocco, with interstation distances close to 60 km. This results in a consistent picture of the crustal variations

beneath the zone. On the other hand, for the Atlas and foreland domains the coverage is still sparse, and future studies will have to test the hypothesis of lateral homogeneity emerging from our data.

[44] **Acknowledgments.** This is a contribution of the Consolider-Ingenio 2010 project TOPO-IBERIA (CSD2006-00041). Additional funding is provided by projects CGL2006-01171, CGL2008-01830, and P09-RNM-5100. We are grateful to the staff of permanent networks to provide relevant data and to all members of the TopoIberia Seismic Working Group for their large effort in the acquisition and processing of field data. The authors thank the useful comments of A. Frassetto and an anonymous referee. We acknowledge work on free software SAC [*Goldstein et al.*, 1999] and GMT [*Wessel and Smith*, 1998].

References

Balanyà, J. C., and V. García-Dueñas (1987), Les directions structurales dans le Domaine d'Alboran de part et d'outre du Détroit de Gibraltar, *C. R. Acad. Sci., Ser. 2*, *304*, 929–933.

Banda, E., J. Gallart, V. García-Dueñas, J. J. Dañobeitia, and J. Makris (1993), Lateral variation of the crust in the Iberian peninsula: New evidence from the Betic Cordillera, *Tectonophysics*, *221*, 53–66.

Calvert, A., E. Sandvol, D. Seber, M. Barazangi, S. Roecker, T. Mourabit, F. Vidal, G. Alguacil, and N. Jabour (2000), Geodynamic evolution of the lithosphere and upper mantle beneath the Alboran region of the western Mediterranean: Constraints from travel time tomography, *J. Geophys. Res.*, *105*(B5), 10,871–10,898, doi:10.1029/2000JB900024.

Cassidy, J. F. (1992), Numerical experiments in broadband receiver function analysis, *Bull. Seismol. Soc. Am.*, *82*, 1453–1474.

Chalouan, A., A. Michard, H. Feinberg, R. Montigny, and O. Saddiqi (2001), The Rif mountain building (Morocco): A new tectonic scenario, *Bull. Soc. Geol. Fr.*, *172*(5), 603–616.

Christensen, N. I. (1996), Poisson's ratio and crustal seismology, *J. Geophys. Res.*, *101*(B2), 3139–3156, doi:10.1029/95JB03446.

Comas, M. C., J. P. Platt, J. I. Soto, and A. B. Watts (1999), The origin and tectonic history of the Alboran Basin: Insights from Leg 161 results, *Proc. Ocean Drill Program Sci. Results*, *161*, 555–579.

Contrucci, I., F. Klingelhoefer, J. Perrot, R. Bartolome, M. A. Gutscher, M. Sahabi, J. Malod, and J. P. Rehault (2004), The crustal structure of the NW Moroccan continental margin from wide-angle and reflection seismic data, *Geophys. J. Int.*, *159*, 117–128, doi:10.1111/j.1365-246X.2004.02391.x.

de Larouzière, F. (1988), The Betic segment of the lithospheric Trans-Alboran shear zone during the late Miocene, *Tectonophysics*, *152*, 41–52, doi:10.1016/0040-1951(88)90028-5.

Diaz, J., J. Gallart, A. Villaseñor, F. Mancilla, A. Pazos, D. Córdoba, J. A. Pulgar, P. Ibarra, and M. Harnafi (2010), Mantle dynamics beneath the Gibraltar Arc (western Mediterranean) from shear-wave splitting measurements on a dense seismic array, *Geophys. Res. Lett.*, *37*, L18304, doi:10.1029/2010GL044201.

Duggen, S., K. Hoernle, and H. van der Bogaard (2004), Magmatic evolution of the Alboran region: The role of subduction in forming the western Mediterranean and causing the Messinian Salinity Crisis, *Earth Planet. Sci. lett.*, *218*, 91–108, doi:10.1016/S0012-821X(03)00632-0.

Efron, B., and R. Tibshirani (1991), Statistical data analysis in the computer age, *Science*, *253*, 390–395.

Faccenna, C., C. Piromallo, A. Crespo-Blanc, L. Jolivet, and F. Rossetti (2004), Lateral slab deformation and the origin of the western Mediterranean arcs, *Tectonics*, *23*, TC1012, doi:10.1029/2002TC001488.

Fadil, A., P. Vernant, S. McClusky, R. Reilinger, F. Gomez, D. B. Sari, T. Mourabit, K. L. Feigl, and M. Barazangi (2006), Active tectonics of the western Mediterranean: GPS evidence for roll back of a delaminated sub-continental lithospheric slab beneath the Rif mountains, *Geology*, *34*, 529–532, doi:10.1130/G22291.1.

Fernández, M., I. Márzan, and M. Torne (2004), Lithospheric transition from the Variscan Iberian Massif to the Jurassic oceanic crust of the central Atlantic, *Tectonophysics*, *386*, 97–115, doi:10.1016/j.tecto.2004.05.005.

Frederiksen, A. W., and M. G. Bostok (2000), Modelling teleseismic waves in dipping anisotropic structures, *Geophys. J. Int*, *141*, 401–412.

Fullea, J., M. Fernàndez, H. Zeyen, and J. Vergés (2007), A rapid method to map the crustal and lithospheric thickness using elevation, geoid anomaly and thermal analysis. Application to the Gibraltar Arc System, Atlas Mountains and adjacent zones, *Tectonophysics*, *430*, 97–117, doi:10.1016/j.tecto.2006.11.003.

Fullea, J., M. Fernàndez, J. C. Alonso, J. Vergés, and H. Zeyen (2010), The structure and evolution of the lithosphere-asthenosphere boundary beneath the Atlantic-Mediterranean transition region, *Lithos*, *120*, 74–95, doi:10.1016/j.lithos.2010.03.003.

Giese, P., and V. Jacobshagen (1992), Inversion tectonics of intracontinental ranges: High and Middle Atlas, Morocco, *Geol. Rundsch.*, *81*(1), 249–259, doi:10.1007/BF01764553.

Goldstein, P., D. Dodge, and M. Firpo (1999), *International Handbook of Earthquake and Engineering Seismology: Part B*, Elsevier, New York.

Gutscher, M. A., J. Malod, J. P. Rehault, I. Contrucci, F. Klingelhoefer, L. Mendes-Victor, and W. Spakman (2002), Evidence for active subduction beneath Gibraltar, *Geology*, *30*, 1071–1074.

Hildenbrand, T. G., R. P. Kucks, M. F. Hamouda, and A. Bellot (1988), Bouguer gravity map and related filtered anomaly maps of Morocco, *U.S. Geol. Surv. Open File Rep.*, *88-517*.

Jacobshagen, V., K. Görler, and P. Giese (1988), *The Atlas System of Morocco: Studies on Its Geodynamic evolution*, *Lect. Notes Earth Sci.*, vol. 15, pp. 481–499, Springer, New York.

Jaffal, M., F. Klingelhoefer, L. Matias, F. Teixeira, and M. Amrhar (2009), Crustal structure of the NW Moroccan margin from deep seismic data(SISMAR Cruise), *Comptes Rendus Geosciences*, *341*(6), 495–503, doi:10.1016/j.crte.2009.04.003.

Jones, C. H., and R. A. Phinney (1998), Seismic structure of the lithosphere from teleseismic converted arrivals observed at small arrays in the southern Sierra Nevada and vicinity, California, *J. Geophys. Res.*, *103*(B5), 10,065–10,090, doi:10.1029/97JB03540.

Julià, J., C. J. Ammon, and R. B. Herrmann (2003), Evaluation of deep sediment velocity structure in the New Madrid Seismic Zone, *Bull. Seismol. Soc. Am.*, *94*, 334–340.

Langston, C. A. (1979), Structure under Mount Rainier, Washington, inferred from teleseismic body waves, *J. Geophys. Res.*, *84*, 4749–4762.

Ligorria, J. P., and C. J. Ammon (1999), Iterative deconvolution and receiver function estimation, *Bull. Seismol. Soc. Am.*, *89*, 1395–1400.

Lombardi, D., J. Braunmiller, E. Kissling, and D. Giardini (2008), Moho depth and Poisson's ratio in the western-central Alps from receiver functions, *Geophys. J. Int.*, *173*, 249–264.

Lonergan, L., and N. White (1997), Origin of the Betic-Rif mountain belt, *Tectonics*, *16*(3), 504–522.

Lujan, M., A. Crespo-Blanc, and J. C. Balanyà (2006), The flysch trough thrust imbricate (Betic Cordillera): A key element of the Gibraltar Arc orogenic wedge, *Tectonics*, *25*, TC6001, doi:10.1029/2005TC001910.

Makris, J., A. Demnati, and J. Klussmann (1985), Deep seismic soundings in Morocco and a crust and upper mantle model deduced from seismic and gravity data, *Ann. Geophys.*, *3*, 369–380.

Missenard, Y., H. Zeyen, D. Frizon de Lamotte, P. Leturmy, C. Petit, M. Sébrier, and O. Saddiqi (2006), Crustal versus asthenospheric origin of relief of the Atlas Mountains of Morocco, *J. Geophys. Res.*, *111*, B03401, doi:10.1029/2005JB003708.

Morales, J., I. Serrano, A. Jabaloy, Galindo-Zaldivar, D. Zhao, F. Torcal, F. Vidal, and F. Gonzalez-Lodeiro (1999), Active continental subduction beneath the Betic cordillera and Alboran Sea, *Geology*, *27*, 735–738.

Pérouse, E., P. Vernant, J. Chéry, R. Reilinger, and S. McClusky (2010), Active surface deformation and sub-lithospheric processes in the western Mediterranean constrained by numerical models, *Geology*, *38*, 823–826, doi:10.1130/G30963.1.

Platt, J. P., S. Allerton, A. Kirker, C. Mandeville, A. Mayfield, E. S. Platzman, and A. Rimi (2003), The ultimate arc: Differential displacement, oroclinal bending, and vertical axis rotation in the external Betic-Rif arc, *Tectonics*, *22*(3), 1017, doi:10.1029/2001TC001321.

Platt, J. P., R. Anczkiewicz, J. I. Soto, S. P. Kelley, and M. Thirlwall (2006), Early Miocene continental subduction and rapid exhumation in the western Mediterranean, *Geology*, *34*, 981–984.

Pollack, H. N., S. J. Hurter, and J. R. Johnson (1993), Heat flow from the Earth's interior: Analysis of the global data set, *Rev. Geophys.*, *31*(3), 267–280, doi:10.1029/93RG01249.

Rimi, A., A. Chalouan, and L. Bahi (1998), Heat flow in the westernmost part of the Alpine Mediterranean system (the Rif, Morocco), *Tectonophysics*, *285*, 135–146, doi:10.1016/S0040-1951(97)00185-6.

Sandvol, E., D. Seber, A. Calvert, and M. Barazangi (1998), Grid search modeling of receiver functions: Implications for crustal structure in the Middle East and North Africa, *J. Geophys. Res.*, *103*(B11), 26,899–26,917, doi:10.1029/98JB02238.

Seber, D., M. Barazangi, A. Ibenbrahin, and A. Demnati (1996), Geophysical evidence for lithospheric delamination beneath the Alboran Sea and the Rif-Betic mountains, *Nature*, *379*, 785–790.

Seber, D., E. Sandvol, C. Sandvold, C. Brindisi, and M. Barazangi (2001), Crustal model for the Middle East and North Africa region: Implications for isostatic compensation mechanism, *Geophys. J. Int.*, *147*, 630–638.

Stich, D., E. Serpelloni, F. Mancilla, and J. Morales (2006), Kinematics of the Iberia-Maghreb plate contact from seismic moment tensors and

GPS observations, *Tectonophysics*, *146*, 295–317, doi:10.1016/j.tecto.2006.08.004.

Tadili, B., M. Ramdani, D. B. Sari, K. Chapochnikov, and A. Bellot (1986), Structure de la croûte dans le nord du Maroc, *Ann. Geophys.*, *4*, 99–104.

Tahayt, A., et al. (2008), Mouvements actuels des blocs tectoniques dans l'arc Bético-Rifain à partir des mesures GPS entre 1999 et 2005, *Geocience*, *340*, 400–413, doi:10.1016/j.crte.2008.02.003.

Teixell, A., M.-L. Arboleya, M. Julivert, and M. Charroud (2003), Tectonic shortening and topography in the central High Atlas (Morocco), *Tectonics*, *22*(5), 1051, doi:10.1029/2002TC001460.

Teixell, A., P. Ayarza, H. Zeyen, M. Fernàndez, and M. L. Arboleya (2005), Effects of mantle upwelling in a compressional setting: The Atlas Mountains of Morocco, *Terra Nova*, *17*, 456–461, doi:10.1111/j.1365-3121.2005.00633.x.

Torne, M., M. Fernàndez, M. C. Comas, and J. I. Soto (2000), Lithospheric structure beneath the Alboran Basin: Results from 3D gravity modeling and tectonic relevance, *J. Geophys. Res.*, *105*(B2), 3209–3228, doi:10.1029/1999JB900281.

van der Meijde, M., S. van der Lee, and D. Giardini (2003), Crustal structure beneath broad-band seismic stations in the Mediterranean region, *Geophys. J. Int.*, *152*, 729–739.

Vinnik, L. P. (1977), Detection of waves converted from *P* to *SV* in the mantle, *Phys. Earth Planet. Inter.*, *15*, 39–45, doi:10.1016/0031-9201(77)90008-5.

Wessel, P., and W. H. Smith (1998), New, improved version of the Generic Mapping Tool released, *Eos Trans. AGU*, *79*, 579.

Wigger, P., G. Asch, P. Giese, W. D. Heinsohn, S. O. E. Alami, and F. Ramdami (1992), Crustal structure along a traverse across the Middle and High Atlas mountains derived from seismic refraction studies, *Geol. Rundsch.*, *81*(1), 237–248, doi:10.1007/BF01764552.

Zandt, G., and C. J. Ammon (1995), Continental crust composition constrained by measurement of crustal Poisson's ratio, *Nature*, *374*, 152–154.

Zeyen, H., P. Ayarza, M. Fernàndez, and A. Rimi (2005), Lithospheric structure under the western African-European plate boundary: A transect across the Atlas Mountains and the Gulf of Cadiz, *Tectonics*, *24*, TC2001, doi:10.1029/2004TC001639.

Zhu, L., and H. Kanamori (2000), Moho depth variation in southern California from teleseismic receiver functions, *J. Geophys. Res.*, *105*(B2), 2969–2980, doi:10.1029/1999JB900322.

D. Córdoba, Departamento de Geofísica, Universidad Complutense de Madrid, E-28040 Madrid, Spain.

J. Diaz, Institute of Earth Sciences "Jaume Almera," CSIC, E-08028 Barcelona, Spain.

F. Gonzalez-Lodeiro, Departamento de Geodinámica, Universidad de Granada, Campus de Fuentenueva s/n, E-18071 Granada, Spain.

M. Harnafi, Institut Scientifique, Université Mohammed V Agdal, Rabat, Morocco.

P. Ibarra, Instituto Geologico y Minero de Espana, La Calera 1, Tres Cantos, E-28760 Madrid, Spain.

J. Julià, Departamento de Geofisica, Universidade Federal do Rio Grande do Norte, Natal, Brazil.

F. de L. Mancilla, J. Morales, and D. Stich, Instituto Andaluz de Geofísica, Universidad de Granada, Profesor Clavera 12, Campus Universitario de Cartuja, E-18071, Granada, Spain. (florlis@ugr.es)

A. Pazos, Real Observatorio de La Armada, E-11100 Cadiz, Spain.

J. A. Pulgar, Departamento de Geología, Universidad de Oviedo, E-33007 Oviedo, Spain.